SPANDIDOS PUBLICATIONS

ONCOLOGY LETTERS 27: 88, 2024

Identification and validation of prognostic genes and immune landscape signatures based on a fatty acid oxidation-related risk score model in glioma

FANGZHOU GUO[1,2], GUOYUAN LING[1,2], ZHENZHU ZHAI[3,4], YI LEI[2], LIGEN MO[2] and HAOZHE PIAO[3]

[1]Graduate School, The Second Affiliated Hospital, Dalian Medical University, Dalian, Liaoning 116000; [2]Department of Neurosurgery, Guangxi Medical University Cancer Hospital, Nanning, Guangxi Zhuang Autonomous Region 530021; [3]Department of Neurosurgery, Liaoning Cancer Hospital and Institute; [4]The First Clinical College, Liaoning University of Traditional Chinese Medicine, Shenyang, Liaoning 110801, P.R. China

Received September 13, 2023; Accepted December 4, 2023

DOI: 10.3892/ol.2024.14222

Abstract. Fatty acid oxidation (FAO) plays a crucial role in glioma metabolism and its interaction with the immune microenvironment. The aim of the present study was to investigate the relationship between FAO-related genes and glioma by constructing gene clusters using a glioma cohort. A total of 287 differentially expressed genes related to FAO were identified and the top 50 genes were selected based on their P-values. Subsequently, patients were classified into two distinct gene subtypes (A and B) based on these genes. Scores for each patient were calculated using the 50 genes and the patients were divided into the high and low-score groups accordingly. Patients in subtype B exhibited higher tumor grades and poor prognostic factors such as older age and worse survival rates. The high-score subgroup had unfavorable indicators, including isocitrate dehydrogenase 1 wild-type, high tumor grade and 1p19q non-codeleted, while immune checkpoint expression was generally higher in the high-score subgroup. The constructed scoring model was validated using an external dataset, and the tissue inhibitor of metalloproteinase 1 gene was identified through protein interaction analysis, suggesting its potential involvement in glioma malignancy and promotion of glioblastoma proliferation. In conclusion, FAO-related genes may contribute to tumor development through immune mechanisms and the present study may provide novel insights for potential therapeutic strategies in glioma treatment.

Correspondence to: Dr Haozhe Piao, Department of Neurosurgery, Liaoning Cancer Hospital and Institute, 44 Xiaoheyan Road, Dadong, Shenyang, Liaoning 110801, P.R. China
E-mail: phzcancerhosp@163.com

Abbreviations: DEGs, differentially expressed genes; EdU, 5-ethynyl-2-doxyuridine; FA, fatty acid; FAO, fatty acid oxidation; GBM, glioblastoma; GO, Gene Ontology; HSG, high score group; IC_{50}, half maximal inhibitory concentration; KEGG, Kyoto Encyclopedia of Genes and Genomes; LGG, low-grade glioma; LSG, low score group; PCA, principal component analysis; ROS, reactive oxygen species; TIMP1, tissue inhibitor of metalloproteinase 1; WB, western blotting; siRNA, small interfering RNA; si-NC, negative control siRNA

Key words: glioma, fatty acid oxidation, prognostic, immune landscape, *TIMP1*

Introduction

Glioma is the most common primary malignant brain tumor in adults worldwide, often affecting individuals 55-60 years of age (1). Gliomas are characterized by diffuse infiltrative growth and high invasiveness, making complete surgical resection challenging and yielding suboptimal outcomes following postoperative traditional chemotherapy with radiotherapy (2,3). Compared with low-grade gliomas (LGGs) (grades II and III), glioblastoma (GBM) (grade IV) is significantly more fatal to patients (4). Patients diagnosed with GBM have a median survival time of <15 months and a 5-year survival rate of <5% (5). Despite current therapies such as anti-angiogenic drugs and electric field therapy, recent therapeutic advances have not yielded substantial benefits, and disease control has remained elusive (6-8). Thus, studying tumorigenesis mechanisms to identify new therapeutic targets is critical (9).

Glioma, as with a number of other rapidly proliferating tumor cells, requires abundant energy to thrive (10). Furthermore, tumor cells develop metabolic pathways to increase the synthesis and transformation of carbohydrates, lipids and proteins (11,12). Changes in tumor metabolism are closely associated with the tumor microenvironment (TME) and immunity (13). The enhanced fatty acid (FA) metabolism observed in glioma is a hallmark of cancer, with the FA composition of cell membranes playing a crucial role in cell survival, lipid peroxidative damage protection and the prevention of ferroptosis (14). Glioma cells derive FAs from exogenous sources or synthesize endogenous FAs excessively through adipogenic pathways (15). Previous studies have found an association between FA oxidation (FAO) and glioma prognosis and malignancy (16-18). However, there has not been an extensive exploration of the link between FA metabolism

and tumor immunity. Therefore, the present study aimed to analyze a prognostic model of FAO-related genes in glioma and its association with tumor immune infiltration, identify a new model and screen out key molecular markers, to facilitate the development of improved therapeutic strategies based on clinical and immune characteristics and treatment responses.

Materials and methods

Data sources. RNA sequencing and clinical data were extracted from The Cancer Genome Atlas (TCGA; https://tcga-data.nci.nih.gov/) LGG and GBM datasets and the Chinese Glioma Genome Atlas (CGGA; http://www.cgga.org.cn/) database (CGGA.mRNAseq_693) (19). A total of 1,363 glioma samples, including 670 from TCGA and 693 from the CGGA were included in the present study. The FAO-related gene signature comprised of 15 genes was determined using the gene set, 'GOBP_POSITIVE_REGULATION_OF_FATTY_ACID_OXIDATION', in the MsigDB database (https://www.gsea-msigdb.org/gsea/msigdb) (20). The genes included PPARG coactivator 1 α, carnitine palmitoyltransferase 1A, mitoregulin, AKT serine/threonine kinase 2, ATP binding cassette subfamily D member 1 (*ABCD1*), fatty acid binding protein 1, *ABCD2*, malonyl-CoA decarboxylase, insulin receptor substrate 1 *(IRS1),* perilipin 5, peroxisome proliferator activated receptor α, peroxisome proliferator activated receptor δ, twist family bHLH transcription factor 1, nuclear receptor subfamily 4 group A member 3 and *IRS2*. The subsequent analysis was performed using the R software (version 4.1.1) (21).

Single-cell level analysis. The expression of FAO-related genes in glioma were analyzed at the single-cell level using the Tumor Immune Single-cell Hub 2 (TISCH2) database (http://tisch.comp-genomics.org/) (22). Furthermore, analyses were conducted to investigate the features and traits of the FAO-related genes located within glioma. The Gene Set Cancer Analysis (GSCA) database (http://bioinfo.life.hust.edu.cn/GSCA/) (23) was used for these additional analyses, which included gene mutation, DNA methylation, somatic copy number variation and immune cell infiltrate analyses.

Principal component analysis (PCA). The present study utilized two R packages, 'sva' and 'limma', to remove batch effects and normalize samples obtained from the TCGA and CCGA databases. PCA was conducted using two R packages, 'FactoMineR' and 'factoextra' to visualize the principle components. A correlation analysis was conducted to determine the correlation between genes using the R package, 'ggplot2'. Additionally, the R package, 'survival', was used to analyze the relationship between FAO-related gene expression and prognostic values in patients with glioma. The R package, 'TSHRC', was used to generate Kaplan-Meier (KM) survival curves, which uses the two-stage test to generate P-values. $P<0.05$ was considered to indicate a statistically significant difference.

Consensus clustering analysis. For exploring the functions of FAO-related genes in glioma, unsupervised consensus cluster analysis was conducted using the 'ConsensusClusterPlus' package in R, which classified patients into different clusters based on the comparison of FAO-related gene expression profiles. Survival analyses were undertaken for each cluster by utilizing the 'survival' and 'survminer' R packages. The 'limma' R package was utilized to analyze the differential expression of FAO-related genes between different clusters. The correlation of gene expression patterns with clinicopathological characteristics were presented as a heatmap using the 'pheatmap' R package. To identify the enriched biological pathways in FAO-related gene sets, the HALLMARK, Kyoto Encyclopedia of Genes and Genomes (KEGG) and Reactome gene sets were downloaded from the Molecular Signature Database, MsigDB 3.0 (http://www.broadinstitute.org/gsea/msigdb/index.jsp). The enrichment of specific biological pathways was then analyzed utilizing the R package, 'GSEA'. The resulting data from the gene set enrichment analysis (GSEA) was used to create a heatmap that compared the enrichment across clusters using the R package 'pheatmap'.

Gene subgroup construction. The R package 'limma' was used for differential expression analysis,, and the R package, 'ggplot2', was utilized to visualize pairwise comparisons via Volcano plots. The screening threshold applied for identifying differentially expressed genes (DEGs) was log fold change >2 and $P<0.05$. The overlapping set of the three differential results was obtained and analyzed further utilizing the R package, 'clusterprofiler', for enrichment analysis. KEGG pathway and Gene Ontology (GO) enrichment analyses were conducted using the R packages, 'enrichplot' and 'ggplot2'.

Gene subgroup immune infiltration. PCA was conducted using the R package, 'prcomp', with default parameters. The R package, 'ESTIMATE', was used to estimate immune infiltration based on the StromalScore, ImmuneScore and ESTIMATEScore and the differences were compared between the subgroups. Furthermore, the infiltration levels of the immune cell types were estimated using the single-sample (ss)GSEA method via the R package, 'GSVA', and the differences were compared between the different subgroups. Finally, all results were visualized using the R package 'ggplot'.

Prognostic scoring model based on key DEGs. To identify a set of candidate prognostic genes, univariate Cox regression analysis was performed using the selected DEGs by R package 'survival' (Table SI). The DEGs were ranked by P-value from high to low, and the top 50 DEGs were selected for unsupervised consensus cluster analysis by R package 'ConsensusClusterPlus'. Survival status, heatmap distribution and differential expression of FAO-related genes were compared between the different DEG subgroups. Following PCA using the top 50 DEGs by R package 'princomp', principal components 1 (PC1) and PC2 were extracted, which were then used to construct the FAO-related DEGs score. The score for each sample was determined based on the prognostic value of the gene signature (24). The formula was as follows: DEGs score=Σ(PC1i)-Σ(PC2i), where 'i' represents DEG expression. Survival analysis was then performed with the 'survival' R package and using KM survival analysis (log-rank test) to compare groups with high and low scores; the cut-off value was determined by using R package 'maxstat' (25). The

relationship between type of cluster, score and prognostic status was displayed in a Sankey diagram, the relationship between FAO gene subtypes, DEG subtypes and scores were separately compared, and the correlation between scores and immune cell infiltration were calculated. The χ^2 test was used to analyze the relationship between the risk score and clinicopathological characteristics of the glioma samples by the 'ggpubr' R package. Additionally, the expression of five immune checkpoints in glioma samples were compared across score subgroups by the R package 'ggpubr'.

Validation set validates scoring model performance. Given the absence of a glioma-specific immunotherapy database and the pan-cancer attributes of immunotherapy, certain datasets containing abundant immunotherapy sample data were selected as validation sets (26-28). The two independent validation datasets, GSE135222 (29) and GSE61676 (30), were downloaded from the Gene Expression Omnibus website (https://www.ncbi.nlm.nih.gov/geo/) (31), to further scrutinize the predictive performance of the deployed scoring model in tumor treatment. Moreover, another validation dataset was obtained from the R package, 'IMvigor210CoreBiologies' (http://research-pub.gene.com/IMvigor210CoreBiologies) (32), which contained a metastatic urothelial tumors cohort. For each sample within the validation sets, the score was calculated using the model constructed in the training set. Next, the risk score, survival rate and recurrence status of the patients were charted to demonstrate the correlation between the risk score and patient response to immunotherapy.

Half maximal inhibitory concentration (IC_{50}) value based on the scoring model. To predict therapeutic response the R package 'pRRophetic' was used to calculate the IC_{50} values of antitumor drugs for each sample. pRRophetic comprises ~700 cell lines and 138 drugs and prognosticates the clinical responsiveness of cancer to specific medications, predicated based on varying gene expression levels in tumors (33,34). The gene expression matrices of these samples were derived from the aforementioned TCGA-LGG and TCGA-GBM datasets. Additionally, the Wilcoxon rank-sum test was used to assess the variability in estimated drug sensitivities between the high score and low score groups. $P<0.05$ was considered to indicate a statistically significant difference.

Screening of key genes through protein-protein interaction (PPI) network construction. The PPI information of the top 50 DEGs was analyzed using the Search Tool for the Retrieval of Interacting Genes (STRING) database (http://www.string-db.org/) and the resulting PPI network was visualized, where the genes represented nodes and the interactions between nodes represented edges. Cytoscape software (v3.7.2) (35). with the plug-in, 'CytoNCA', was then used to select the hub genes from the PPI network. The expression and prognostic correlation of the screened hub gene in different grades of glioma were verified using the GEPIA database (http://gepia.cancer-pku.cn/).

Verification of hub gene expression. The HMC3, HS683, A172 (CRL-1620), LN229 and SF539 cell lines were obtained from the American Type Culture Collection (ATCC). All cell lines were maintained in DMEM (Shanghai Basal Media Technologies Co., Ltd.) containing 10% fetal bovine serum (cat. no. C04001-500; Shanghai VivaCell Biosciences, Ltd.) and 1% penicillin/streptomycin (cat. no. S110B; Shanghai Basal Media Technologies Co., Ltd.), respectively. Protein was extracted from the cells using the RIPA buffer (Beyotime Institute of Biotechnology). The protein expression levels of the hub gene *TIMP1* in various cells were examined using western blotting (WB). The protein concentration was determined with the BCA Protein Assay Kit (Beyotime Institute of Biotechnology). Protein samples were electrophoresed on a 10% gel using SDS-PAGE, with 15 μg per lane, and then transferred to an nitrocellulose membrane (MilliporeSigma). The membrane was then blocked at room temperature for 1 h with 5% skimmed milk/PBS. The tissue inhibitor of metalloproteinase 1 (TIMP1) antibody (cat. no. K101524P) was obtained from Beijing Solarbio Science & Technology and the α-tubulin antibody (cat. no. ER130905) was obtained from Hangzhou HuaAn Biotechnology Co., Ltd. The TIMP1 antibody was diluted 1:1,000 and the α-tubulin antibody was diluted 1:5,000. Samples were incubated with the primary antibodies overnight on a shaker at 4°C. After washing with TBST containing 0.1% Tween, the membranes were incubated with secondary antibodies (anti-Rabbit kit; cat. no. A32732; Invitrogen; Thermo Fisher Scientific, Inc.) for 1 h at room temperature. Protein bands were subsequently visualized using the BeyoECL Star chemiluminescence substrate (cat. no. P0018AM; Beyotime Institute of Biotechnology) under the ChemiDoc Imaging System (Bio-Rad Laboratories, Inc.) and analyzed using ImageJ software (1.47v; National Institutes of Health).

Immunohistochemistry images were downloaded from the Human Protein Atlas (HPA) website (https://www.proteinatlas.org/humanproteome/pathology).

TIMP1 knockdown. The human glioblastoma cell lines, LN229 and SF539, were cultured at 37°C in a 5% CO2 incubator, in High Glucose DMEM (Shanghai Yuanpinghao Biotech Co., Ltd.) containing 10% fetal bovine serum (Shanghai VivaCell Biosciences, Ltd.). Both cell lines were obtained from preserved cells in our laboratory (36), originally purchased from the ATCC. Two small interfering (si) RNAs targeting *TIMP1* and a negative control were designed and synthesized by Guangzhou RiboBio Co., Ltd. The sequences were as follows: si-*TIMP1*-1 (sense, 5'-AGAUGACCAAGAUGUAUAAAG-3'; antisense, 5'-UUAUACAUCUUGGUCAUCUUG-3'); si-*TIMP1*-2 (sense, 5'-CACAGUGUUUCCCUGUUUAUC-3'; antisense, 5'-UAAACAGGGAAACACUGUGCA-3') and si-NC (sense, 5'-UUCUCCGAACGUGUCACGUTT-3'; antisense, 5'-ACGUGACACGUUCGGAGAATT-3'). Lipofectamine 3000 (Thermo Fisher Scientific, Inc.) was used for transfection into the LN229 and SF539 cell lines, according to the manufacturer's instructions.

Colony formation assay. LN229 and SF539 cells were transfected with the *TIMP1* siRNAs or siNC for 48 h as aforementioned. Then, the cells (1,500 cells/well) were inoculated into a 6-well plate and transfected with siRNA again on the 6th day. Given the temporary nature of transient transfection, transfection was performed twice to ensure the knockdown effect of TIMP1. The cells were incubated for a further 6 days when they were washed with PBS and stained with 4%

polyformaldehyde for 40 min, then stained with 0.1% crystal violet for 2 h at room temperature. Colonies with >50 cells were counted using the ImageJ software.

Cell viability. Cell viability was assessed using Cell Counting Kit-8 (CCK-8; APeXBIO Technology LLC; lot no. K101826133EF5E). The siRNA transfected LN229 and SF539 cells (3,000-4,000 cells/well) were seeded into a 96-well plate. Fresh culture medium (100 μl) containing CCK-8 solution (10 μl) was added to each well of the plate in the dark, then the plated was incubated for 2 h in the dark. The absorbance at a wavelength of 450 nm was measured to detect cell viability.

5-ethynyl-2-deoxyuridine (EdU) assay. An EdU kit (BeyoClick™ EDU-488; Beyotime Institute of Biotechnology) was used to detect the effect of *TIMP1* knockdown on GBM cell proliferation. LN229 and SF539 cells transfected with si-*TIMP1* or si-NC for 48 h were co-cultured in EdU working solution (1:1,000) in a 37˚C and 5% CO_2 incubator for 3 h. After incubation, the cells were fixed with 4% paraformaldehyde for 30 min at room temperature, washed and incubated with reaction solution, according to the instruction manual. Then, the cells were treated with Hoechst reagent at room temperature for 10 min to label the cell nuclei. Detection was conducted using a fluorescence microscope (Leica DMi8; Leica Microsystems GmbH), and images were captured using ToupView (v3.7) software (AmScope).

Flow cytometry. Cell apoptosis was detected by flow cytometry using the annexin V-FITC/PI Apoptosis Detection Kit (Nanjing KeyGen Biotech Co., Ltd.), with operations performed according to the manufacturer's instructions. The BD FACSCelesta (BD Biosciences) flow cytometer was used for detection, and statistical analysis was conducted using Flow Jo (v10.8.1; FlowJo LLC) software.

Statistical analysis. Each experiment was repeated at least three times independently. Data are presented as the mean ± standard deviation. All statistical analyses were performed using GraphPad Prism (v9.0) software (Dotmatics) with either unpaired Student's t-test or one-way ANOVA with Bonferroni's adjustment. P<0.05 was considered to indicate a statistically significant difference.

Results

Genetic mapping and epigenetic landscape of glioma. In the present study, the genetic mapping and epigenetic landscape of glioma were examined by investigating 13 FAO-related genes. Using TISCH analysis, the single-cell expression of FAO-related genes in glioma were observed (Fig. S1). The analysis of somatic mutations demonstrated a higher frequency of mutations in the GBM cohort than in the LGG cohort (Fig. 1A). Furthermore, the distribution of mutations in the top 10 mutated genes in glioma were summarized, along with their copy number variations (CNVs) and the ratio of somatic mutations (Fig. 1B). A total of 30 samples with complete single-cell information were obtained from the 'glioma' dataset on the TISCH2 website. Of the 30 samples analyzed, 28 had various genetic alterations, including missense mutations, frame shift insertions and multi-hit mutations. Fig. 2A shows the distribution of the frequency of harmful mutations in FAO-related genes in gliomas. Specifically, a positive correlation between CNVs and mRNA expression levels was found, while a negative correlation between methylation levels and mRNA expression levels was observed (Fig. 2B-D). The genetic landscape and expression levels of FAO-related genes were significantly different between different grades of glioma, indicating a potential function of FAO-related genes in glioma initiation and malignancy. Finally, the FAO-related genes show a strong correlation with various immune cells, and this correlation is more pronounced in LGG, suggesting a potential connection between FAO-related genes and glioma immune infiltration (Fig. S2).

Identification of FAO-related genes clusters in glioma. After performing PCA analysis and visualization, a total of 15,803 genes and 1,363 samples were obtained from LGG and GBM in the TGGA and CCGA cohorts (Fig. 3A). Following survival analysis, the KM survival curves demonstrated that the expression of 11 genes was significantly correlated with prognosis (P<0.05; Fig. 3C). Of the 11 genes, high expression of 8 genes was associated with a poor prognosis, and high expression of 3 genes was associated with a good prognosis. Additionally, through network analysis, the complete genetic landscape was visualized, including the regulatory relationship between genes and their prognostic implications in patients with glioma (Fig. 3B).

An unsupervised cluster analysis identified three optimal clusters (k=3), based on the relative change in the area under the cumulative distribution function curve (Fig. 4A). KM curves indicated a poor prognosis for patients in cluster B compared with the other two clusters (P<0.001; Fig. 4B). Notably, certain genes displayed different expression levels within different clusters, which suggested that they may have prognostic significance within the specific cluster (Fig. 4C). Moreover, comparing the clinicopathological features of the different glioma clusters revealed significant differences in the expression of FAO-related genes and clinicopathological features. Cluster B displayed higher World Health Organization grades (III-IV; P<0.01) and an older age (P<0.01) compared with the other two clusters (Fig. 4D).

To further explore the differences between clusters, HALLMARK, KEGG and Reactome pathway data were downloaded from the MsigDB database, revealing significant variations in multiple pathways among pairwise contrasted clusters, such as the p53 signaling pathway, apoptosis pathway, notch signaling pathway and cell cycle (Fig. S3).

Screening DEGs based on the FAO-related genes clusters. Differential analyses were employed to identify three gene subtypes and the results were represented in a volcano plot. By taking the intersection of the DEGs among the three subtypes, 287 candidate DEGs were identified (Fig. 5A). GO and KEGG pathway analyses revealed that the enriched pathways of the DEGs were primarily associated with tumorigenesis and development (Fig. 5B and C). A visual network was constructed to display the relationships between the top 5 DEGs and the KEGG pathways (Fig. 5D).

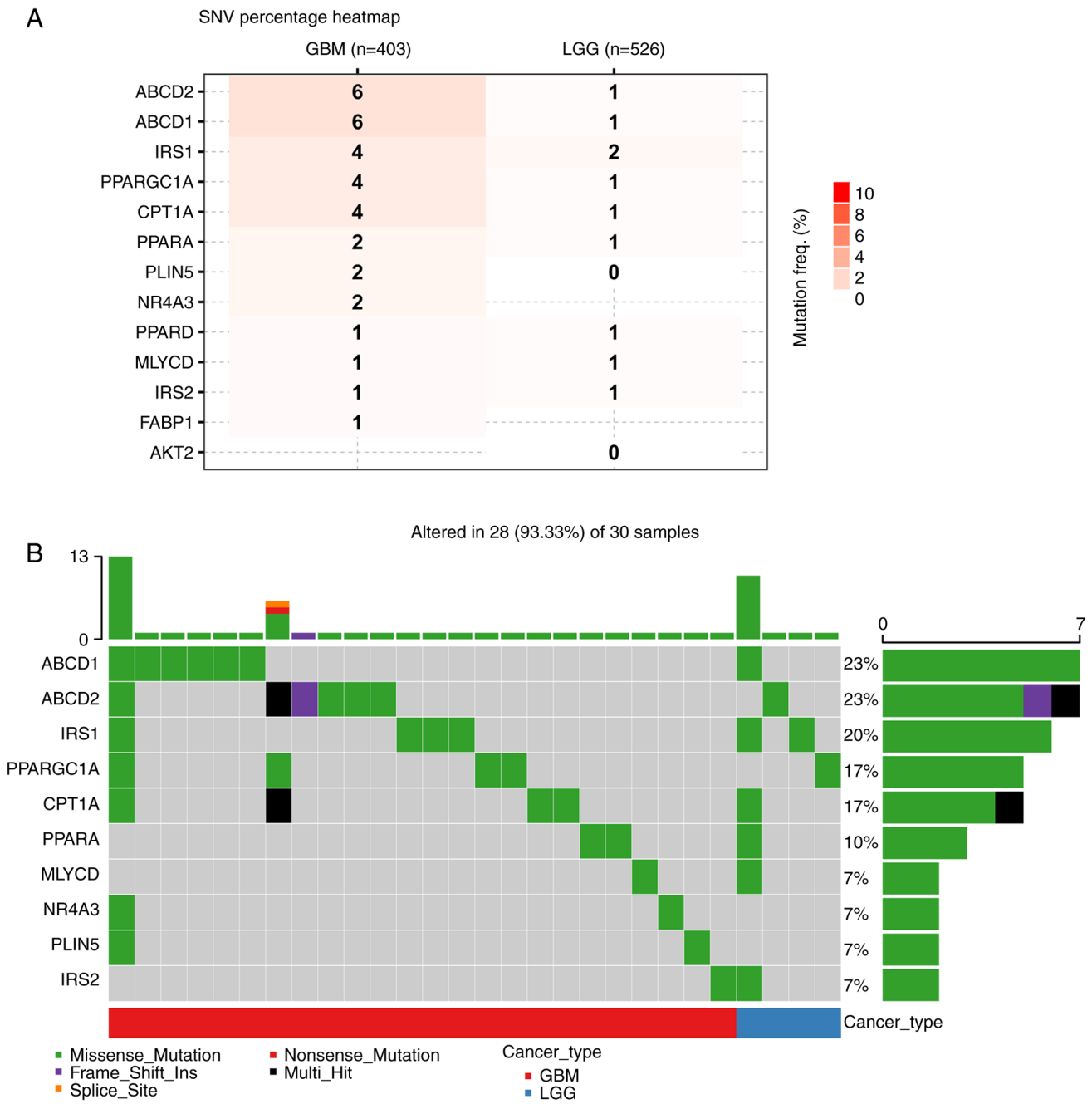

Figure 1. SNV data of FAO-related genes in the glioma cohort from the GSCA database (http://bioinfo.life.hust.edu.cn/GSCA/#/). (A) The SNV frequency of FAO-related genes in the glioma cohort. (B) Summary of the frequency of deleterious mutations in the glioma cohort. SNV, single nucleotide variants; LGG, low grade glioma; GBM, glioblastoma; FAO, fatty acid oxidation; PPARGC1A, PPARG coactivator 1 α; CPT1A, carnitine palmitoyltransferase 1A; MTLN, mitoregulin; AKT2, AKT serine/threonine kinase 2; ABCD1, ATP binding cassette subfamily D member 1; FABP1, fatty acid binding protein 1; ABCD2, ATP binding cassette subfamily D member 2; MLYCD, malonyl-CoA decarboxylase; IRS1, insulin receptor substrate 1; PLIN5, perilipin 5; PPARA, peroxisome proliferator activated receptor α; PPARD, peroxisome proliferator activated receptor δ; TWIST1, twist family bHLH transcription factor 1; NR4A3, nuclear receptor subfamily 4 group A member 3; IRS2, insulin receptor substrate 2.

The subsequent PCA demonstrated significant differences in transcriptional profiles between subtype B and the other two subtypes (Fig. 6A). To assess the TME score, which included the stromal, immune and ESTIMATE scores, for the three gene subtypes, the ESTIMATE package was utilized. A higher stromal or immune score indicated greater proportions of stromal cells or immunocytes in the TME, while the ESTIMATE score reflected the sum of these scores. The findings indicated that patients with subtype B had higher TME scores (Fig. 6B).

To compare immune cell infiltration across the different gene subtypes, the ssGSEA function within the R package, GSVA, was used. Notably, subtype B demonstrated higher immune infiltration compared with the other subtypes, with a marked increase in $CD4^+$ T cells, $CD8^+$ T cells, γδT cells, mast cells, macrophages and regulatory T cells ($P<0.01$; Fig. 6C).

Constructing gene subgroups based on the DEGs. Since gene expression is controlled by a complex regulatory

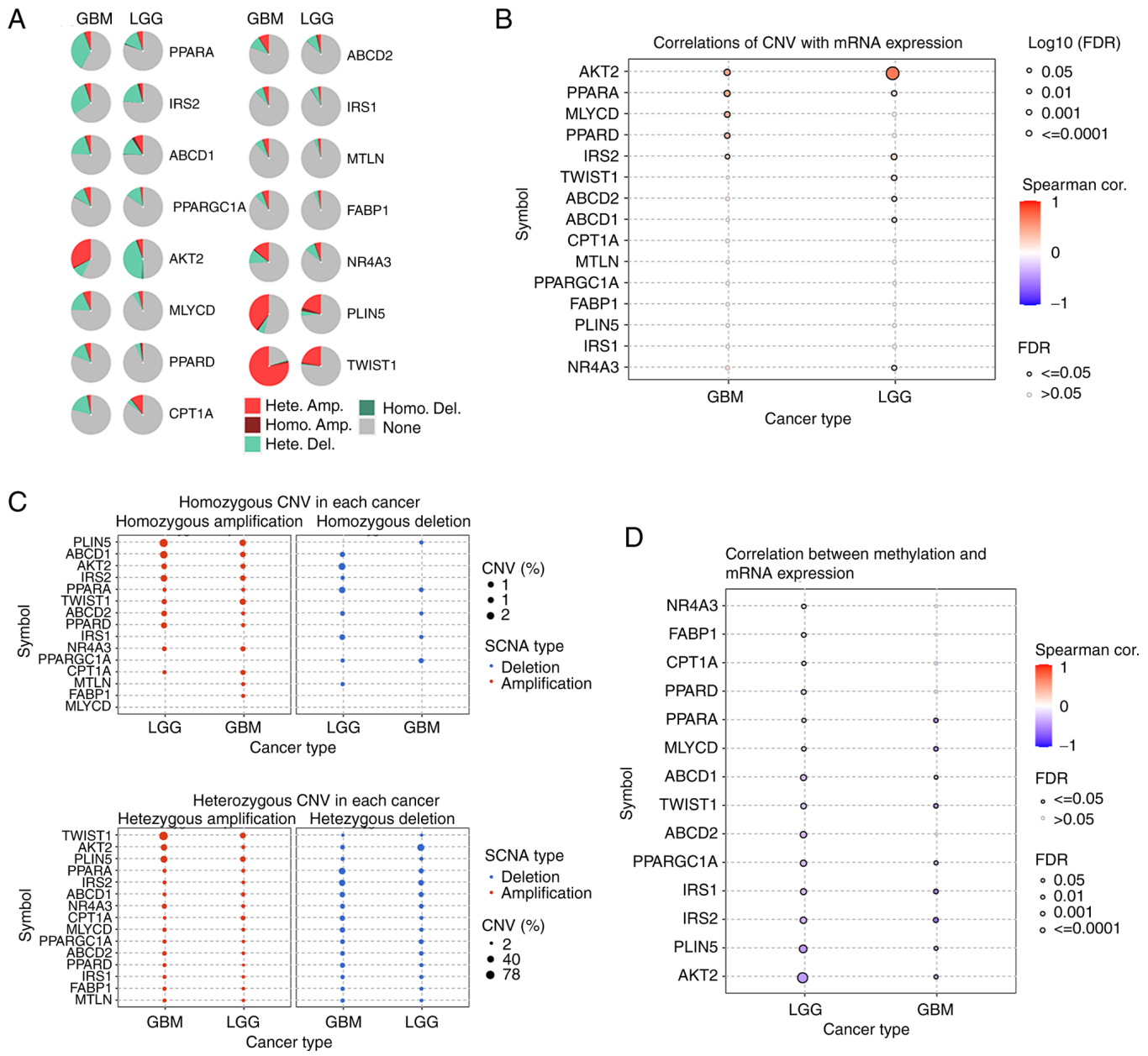

Figure 2. CNV data of FAO-related genes in the glioma cohort from the GSCA database (http://bioinfo.life.hust.edu.cn/GSCA/#/). (A) Pie plots summarizing the CNV of FAO-related genes in the glioma cohort. (B) The correlation between CNV and mRNA expression of FAO-related genes in the glioma cohort. (C) The homozygous and heterozygous CNV profiles of FAO-related genes in the glioma cohort. (D) The correlation between methylation and mRNA expression of FAO-related genes in the glioma cohort. CNV, copy number variation; LGG, low grade glioma; GBM, glioblastoma; FAO, fatty acid oxidation; cor., correlation; Hete., heterozygous; Homo., homozygous; SCNA, somatic copy number; FDR, false discovery rate; PPARGC1A, PPARG coactivator 1 α; CPT1A, carnitine palmitoyltransferase 1A; MTLN, mitoregulin; AKT2, AKT serine/threonine kinase 2; ABCD1, ATP binding cassette subfamily D member 1; FABP1, fatty acid binding protein 1; ABCD2, ATP binding cassette subfamily D member 2; MLYCD, malonyl-CoA decarboxylase; IRS1, insulin receptor substrate 1; PLIN5, perilipin 5; PPARA, peroxisome proliferator activated receptor α; PPARD, peroxisome proliferator activated receptor δ; TWIST1, twist family bHLH transcription factor 1; NR4A3, nuclear receptor subfamily 4 group A member 3; IRS2, insulin receptor substrate 2.

network, the deep connections between genes were further explored based on the screened DEGs. Single-factor regression analysis was conducted using the identified 287 DEGs, which were sorted by P-value, and the top 50 DEGs with the smallest P-values were screened (Fig. S4). These DEGs were subsequently divided into two subgroups based on unsupervised clustering analysis (Fig. 7A). To compare the survival time of the patients in the two groups, the 'survival' and 'survminer' packages in R were utilized. The analysis demonstrated that the survival rate of patients in subgroup A was significantly higher than that in subgroup B (P<0.01; Fig. 7B).

The distribution and clinicopathological characteristics of the DEGs in the two subgroups were visualized using a heat map, which also revealed differences between the two subgroups. Subgroup B was associated with a higher tumor grade and a greater number of patients with isocitrate dehydrogenase ($NADP^+$) (*IDH1*) wild-type (Fig. 7D). Notably, genes related to FAO exhibited significant differences between the two subtypes (Fig. 7E).

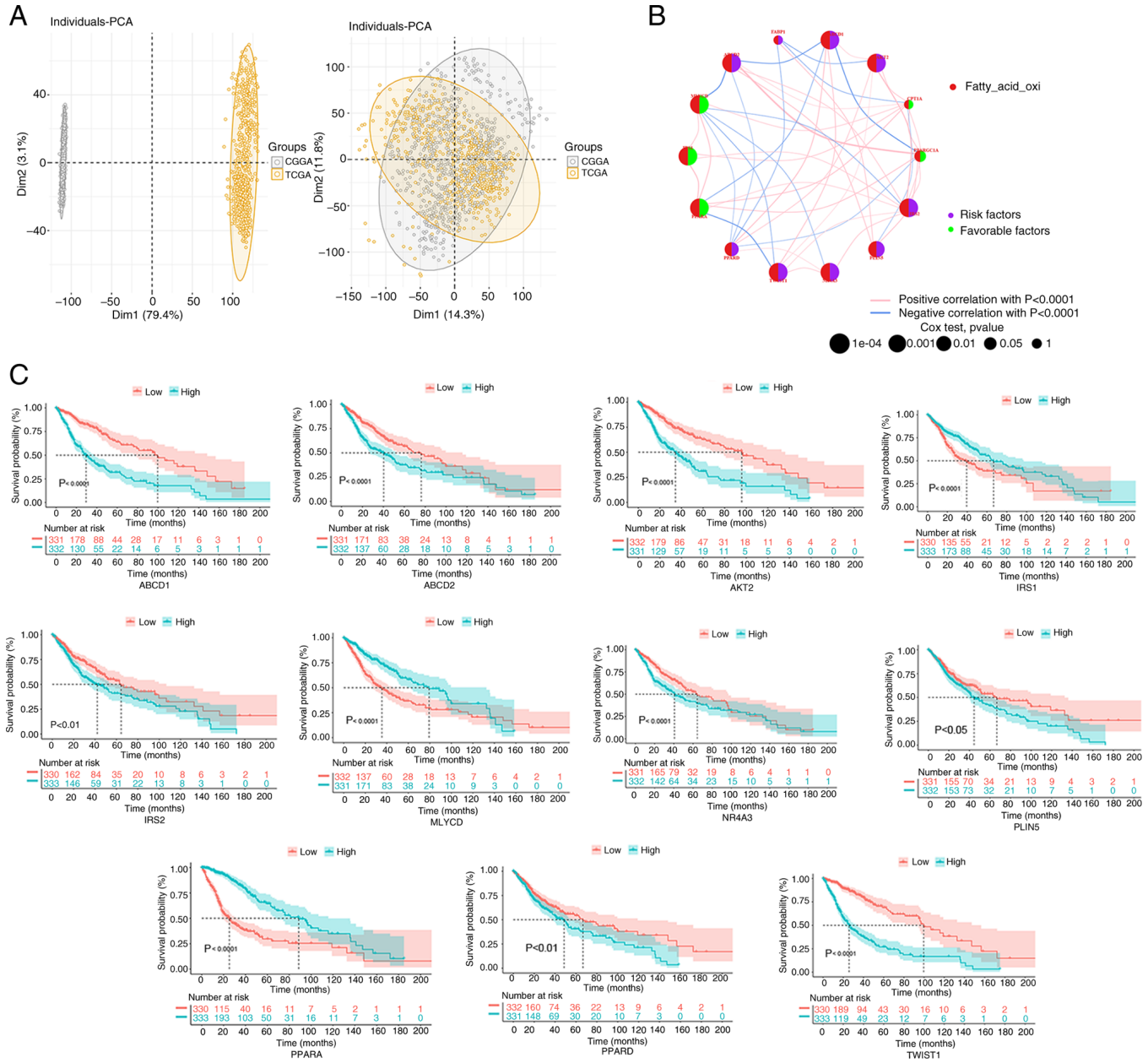

Figure 3. FAO-related gene correlation and prognostic analysis in the glioma cohort. (A) In the PCA, samples from TCGA and CGGA databases were classified. (B) To predict the relationship between FAO-related genes and glioma prognosis, the 'survival' and 'survminer' packages were used to perform the log-rank test and Cox regression analysis. The circle size indicates the P-value, and the lines linking the FAO-related genes indicate their interactions. Circles in purple indicate prognostic risk factors and green circles represent prognostic protective factors. (C) Kaplan-Meier survival curves were used to observe the relationship between FAO-related genes and survival in the integrated samples. CGGA, Chinese Glioma Genome Atlas; FAO, fatty acid oxidation; PCA, principal component analysis; TCGA, The Cancer Genome Atlas; PPARGC1A, PPARG coactivator 1 α; CPT1A, carnitine palmitoyltransferase 1A; AKT2, AKT serine/threonine kinase 2; ABCD1, ATP binding cassette subfamily D member 1; FABP1, fatty acid binding protein 1; ABCD2, ATP binding cassette subfamily D member 2; MLYCD, malonyl-CoA decarboxylase; IRS1, insulin receptor substrate 1; PLIN5, perilipin 5; PPARA, peroxisome proliferator activated receptor α; PPARD, peroxisome proliferator activated receptor δ; TWIST1, twist family bHLH transcription factor 1; NR4A3, nuclear receptor subfamily 4 group A member 3; IRS2, insulin receptor substrate 2.

Construction of a score model based on the PCA. The patients undergoing PCA analysis were divided into the high score group (HSG) and the low score group (LSG) based on the median value. The resultant KM curves indicated that the HSG had a significantly lower survival rate compared with the LSG group (P<0.01; Fig. 8A). Time-dependent receiver operating characteristic curve analysis revealed that the scoring model demonstrated good predictive performance, with area under the curve values of 0.805, 0.848 and 0.817 for 1-, 3- and 5-years, respectively (Fig. 7C). The Sankey plot displayed the distribution of patients in the three FAO-related gene clusters, two gene subgroups and two score groups (Fig. 8B). Notable differences in the distribution of scores among the different groups and gene subgroups were found (Fig. 8C and D). The score values were significantly and positively correlated with immune cell infiltration, with a corresponding distribution shown in Fig. 8E.

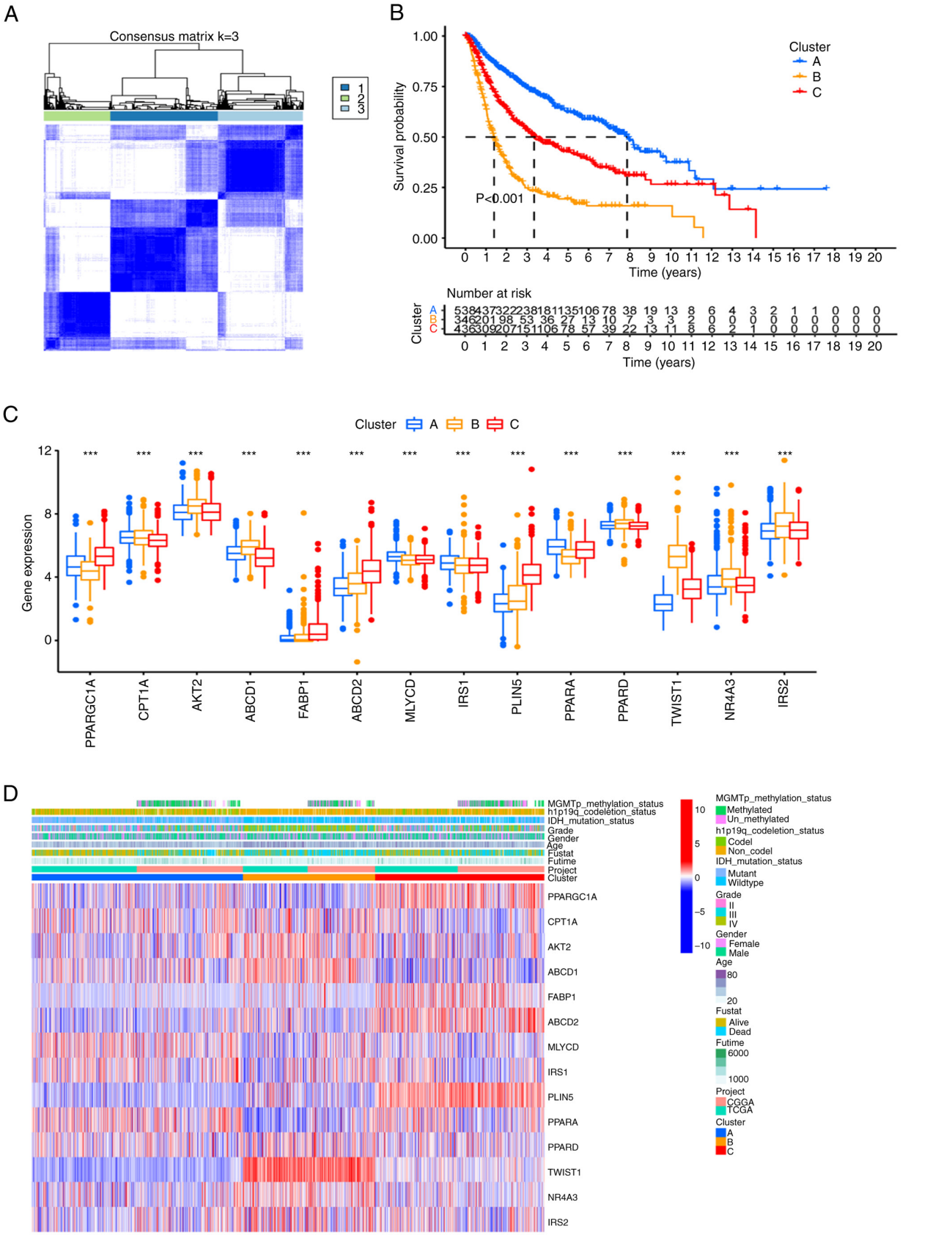

Figure 4. Unsupervised clustering based on the FAO-related gene signature. (A) The samples were clustered into different subgroups by unsupervised clustering. The most suitable value of k is k=3. (B) Prognostic Kaplan-Meier curves for the 3 clusters. (C) Differential expression of FAO-related genes among the 3 clusters. (D) Heat map of the clinicopathological characteristics and gene phenotypes in the 3 clusters. ***P<0.001. CGGA, Chinese Glioma Genome Atlas; FAO, fatty acid oxidation; TCGA, The Cancer Genome Atlas; PPARGC1A, PPARG coactivator 1 α; CPT1A, carnitine palmitoyltransferase 1A; AKT2, AKT serine/threonine kinase 2; ABCD1, ATP binding cassette subfamily D member 1; FABP1, fatty acid binding protein 1; ABCD2, ATP binding cassette subfamily D member 2; MLYCD, malonyl-CoA decarboxylase; IRS1, insulin receptor substrate 1; PLIN5, perilipin 5; PPARA, peroxisome proliferator activated receptor α; PPARD, peroxisome proliferator activated receptor δ; TWIST1, twist family bHLH transcription factor 1; NR4A3, nuclear receptor subfamily 4 group A member 3; IRS2, insulin receptor substrate 2.

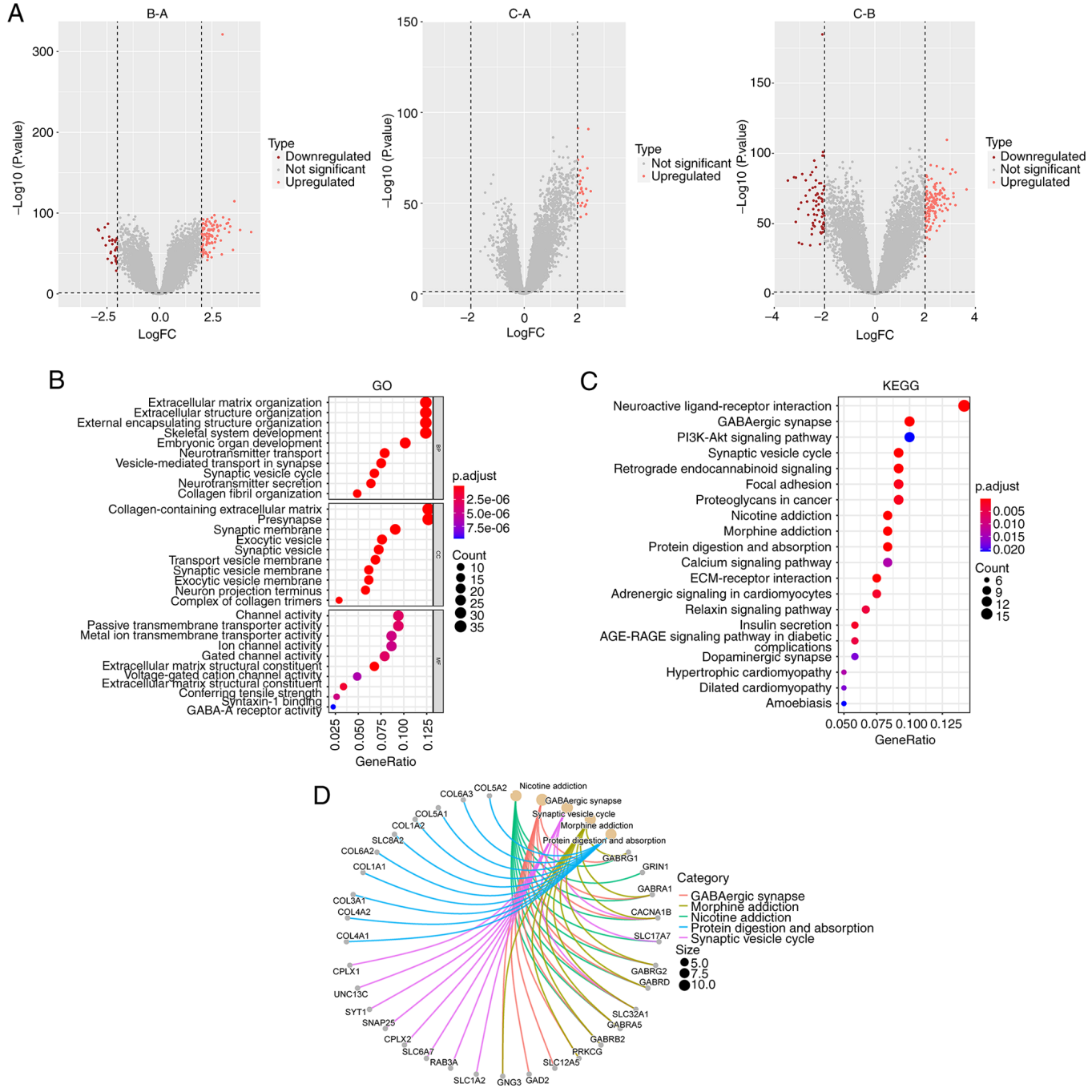

Figure 5. Differential gene selection. (A) Volcano plots of the DEGs based on differential expression analysis. (B) GO and (C) KEGG analysis of the obtained 287 DEGs following differential analysis. (D) The relationship between the genes and pathways in the top 5 KEGG results. The size of the circle represents the strength of the relationship between genes and pathways, the larger the size, the stronger the correlation. DEGs, differentially expressed genes; GO, Gene Ontology; KEGG, Kyoto Encyclopedia of Genes and Genomes.

It was observed that the survival status was diminished in the HSG, and that the HSG showed poor characteristics, including higher grade, older age, *IDH1* wild-type, 1p19q non-co-deletion and other poor prognostic factors (Fig. 9A-F). These differences were statistically significant (P<0.01). A total of five immune checkpoints, including programmed cell death 1 ligand 1, Lymphocyte activation gene 3 protein, programmed cell death protein 1, cytotoxic T-lymphocyte protein 4 and T-cell immunoreceptor with Ig and ITIM domains, were selected for analysis and it was found that immune checkpoints were generally upregulated in the HSG (Fig. 10A). We hypothesize that the HSG has enhanced sensitivity to immunotherapy and is more conducive to treatment using immunosuppressants.

Assessing score model performance using the validation sets. To evaluate the score model, it was verified using external datasets, including GSE135222 (patients with advanced non-small cell lung carcinoma) and GSE61676 (patients with late-stage non-squamous non-small cell lung cancer), and the IMvigor210CoreBiologies package. In the three validation datasets, the KM curves showed that the survival rate of the

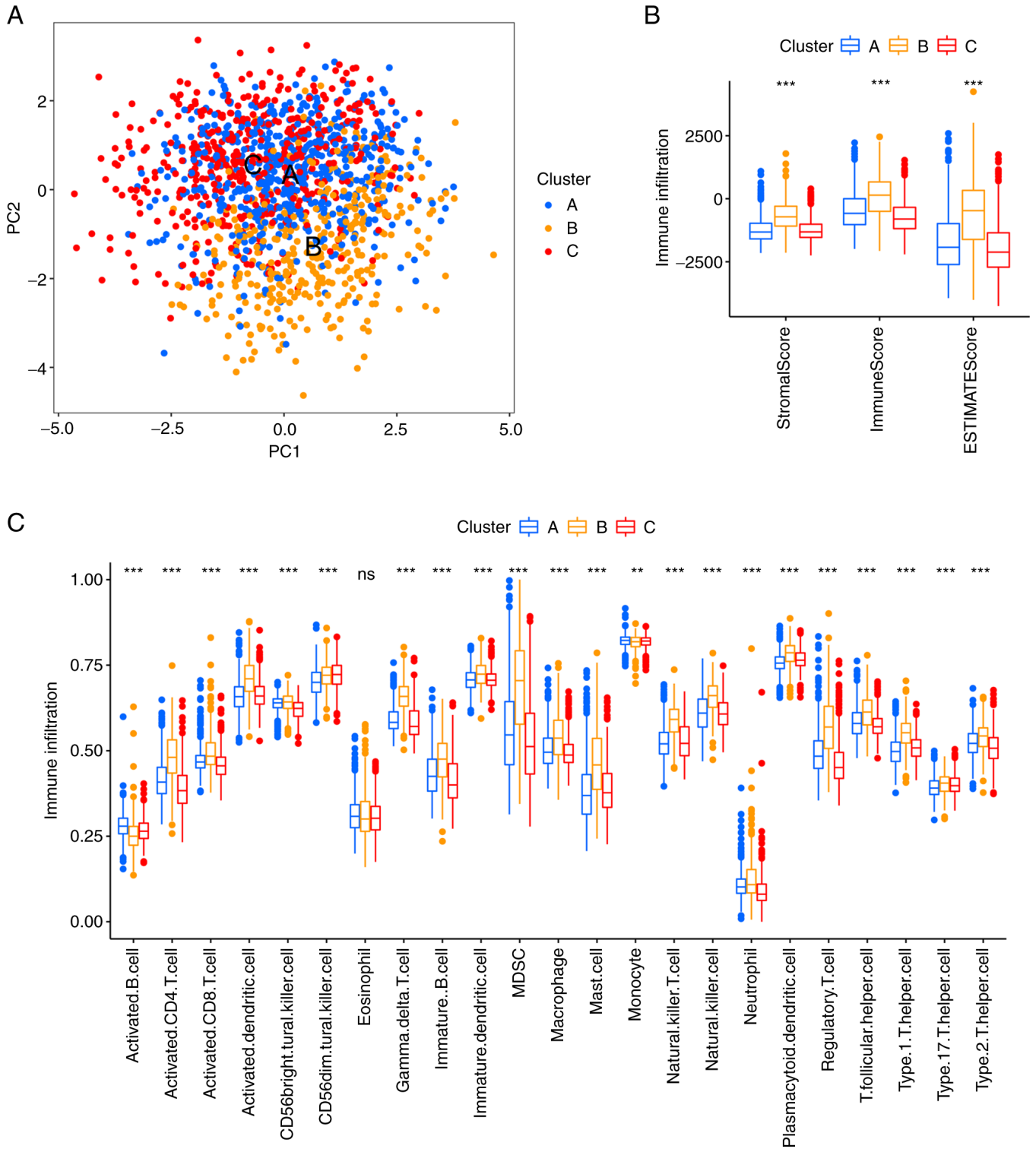

Figure 6. Relationship between the clusters and immune cell infiltration. (A) PCA was used to compare the differences among all clusters. (B) The expression scores of different clusters included in the ESTIMATE algorithm for determination of stromal and immune gene signatures. (C) The differences in the infiltration of 23 immune cells between clusters using single-sample Gene Set Enrichment Analysis. **P<0.01; ***P<0.001. PCA, principal component analysis; ns, not significant.

HSG was better than that of the LSG (P<0.01). In addition, in the GSE135222 dataset, the tumor progression rate of the HSG was lower (P<0.05). In the GSE61676 dataset, the HSG seemed to have a higher rate of immune therapy response. In the IMvigor210 dataset, the rate of remission for tumor appeared to be higher in the HSG (Fig. 10B-D). The aforementioned results indicated that the score model could be applied to other tumors and be beneficial for the immunosuppressive treatment of glioma.

The differences in the effectiveness of various immunosuppressants between the HSG and the LSG were analyzed by comparing the IC_{50} values. The Wilcoxon rank-sum test was

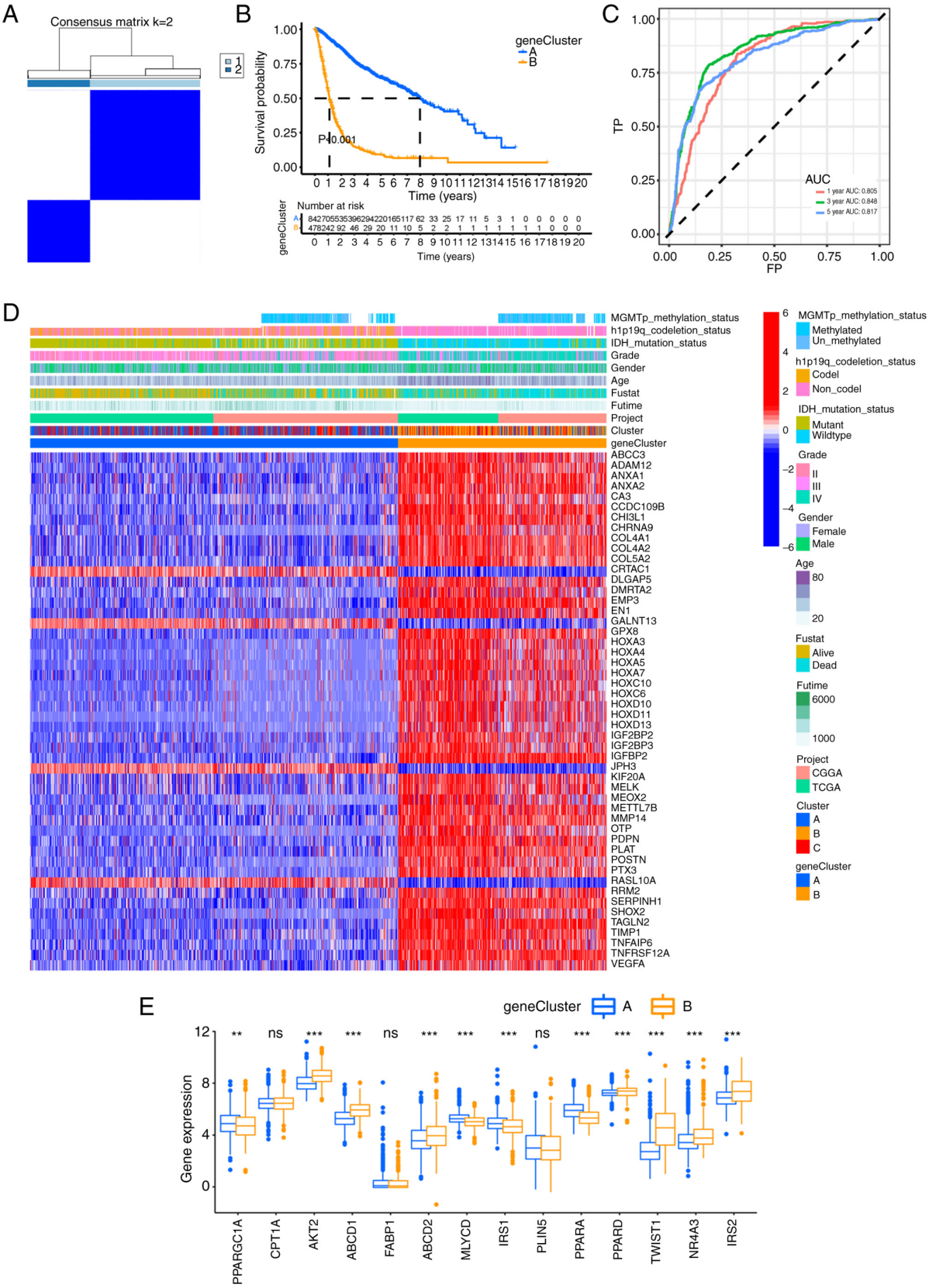

Figure 7. Consensus clustering and risk scoring model construction for the top 50 DEGs. (A) Clustering of the top 50 DEGs. The optimal number of clusters was k=2. (B) Kaplan-Meier survival curve of the gene subtypes based on the top 50 DEGs. (C) Receiver operating characteristic curve of the risk score model. (D) Heat map illustrating the differences in the DEG expression profiles and the clinicopathological characteristics between two gene subtypes in the glioma cohort. (E) Differential expression of fatty acid oxidation-related genes between the two gene subtypes. **P<0.01; ***P<0.001. AUC, area under the curve; CGGA, Chinese Glioma Genome Atlas; DEGs, differentially expressed genes; ns, not significant; TCGA, The Cancer Genome Atlas; PPARGC1A, PPARG coactivator 1α; CPT1A, carnitine palmitoyltransferase 1A; AKT2, AKT serine/threonine kinase 2; ABCD1, ATP binding cassette subfamily D member 1; FABP1, fatty acid binding protein 1; ABCD2, ATP binding cassette subfamily D member 2; MLYCD, malonyl-CoA decarboxylase; IRS1, insulin receptor substrate 1; PLIN5, perilipin 5; PPARA, peroxisome proliferator activated receptor α; PPARD, peroxisome proliferator activated receptor δ; TWIST1, twist family bHLH transcription factor 1; NR4A3, nuclear receptor subfamily 4 group A member 3; IRS2, insulin receptor substrate 2.

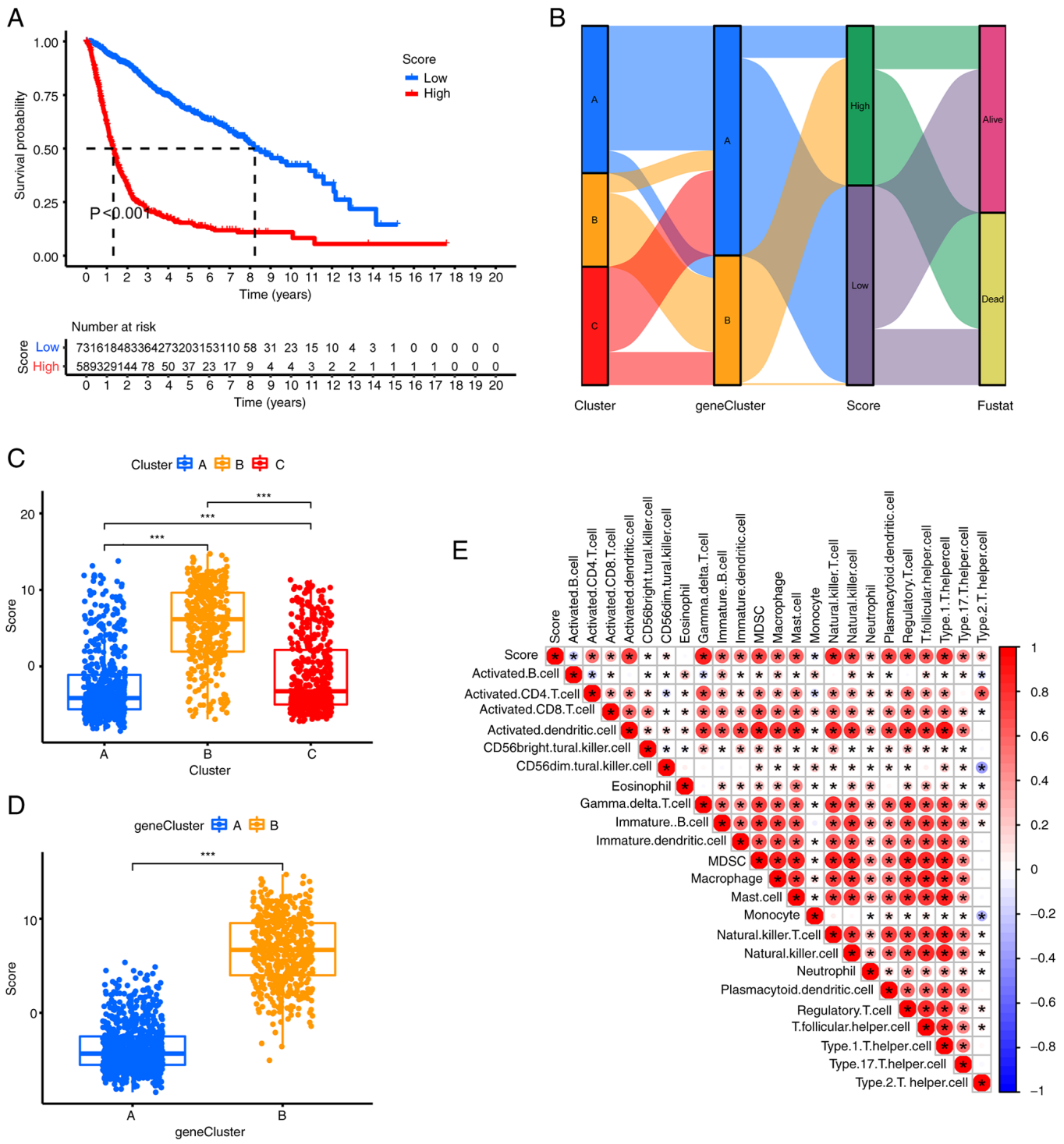

Figure 8. Assessment of the relevance of the risk scores and clustering. (A) Kaplan-Meier curve analysis of the high and low-score groups. (B) Sankey diagram demonstrating the association between clusters, gene clusters, score groups and the prognostic signature. (C) Significant differences in the scores of different clusters based on the 287 differentially expressed genes. (D) Significant differences in the scores of different gene clusters. (E) Correlation analysis of risk score and immune cell infiltration. Red represents positive correlation, blue represents negative correlation; the darker the color, the stronger the correlation. ***P<0.001.

employed to determine the statistical differences between the two groups (Fig. S5).

Screening and experimental validation of a key gene. The PPI network analysis revealed that *TIMP1* is a key gene in glioma (Fig. 11A). Subsequent GEPIA analysis indicated a significant upregulation of *TIMP1* in high-grade glioma compared with normal brain tissue (P<0.05; Fig. 11F), but no significant difference in low-grade glioma compared with normal brain tissue. High *TIMP1* expression was associated with poor prognosis and increased risk of suboptimal disease-free survival and overall survival rates in patients with glioma (P<0.01; Fig. 11B). Furthermore, results from the WB experiments corroborated this finding, demonstrating high

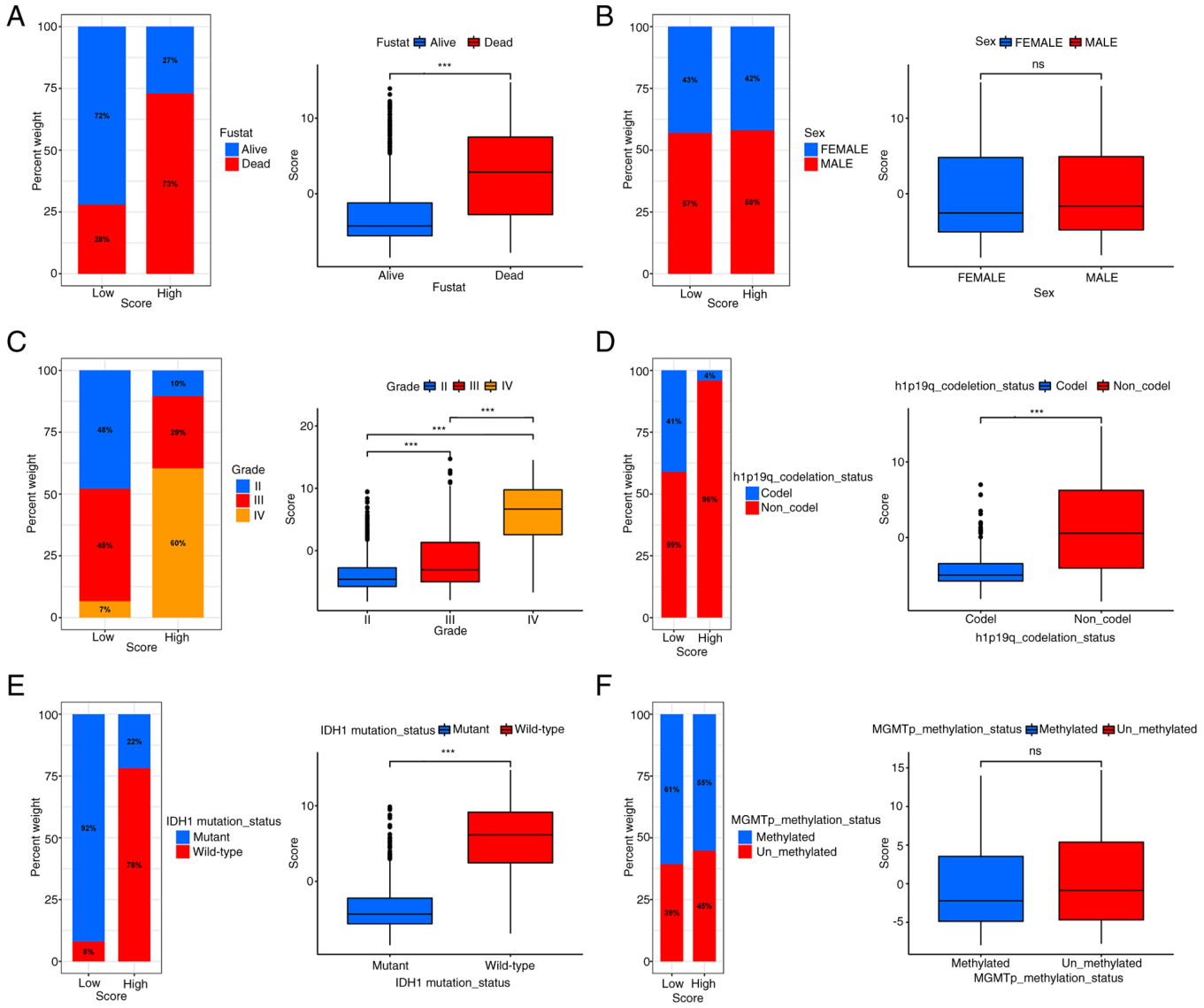

Figure 9. Relationship between the risk score model and different clinicopathological characteristics. Relationship between the risk score model and (A) survival status, (B) sex, (C) grade, (D) 1p19q codeletion status, (E) IDH1 and (F) MGMTp methylation. ***P<0.001; ns, not significant. IDH1, isocitrate dehydrogenase 1; MGMTp, methylguanine-DNA methyltransferase.

TIMP1 protein expression in all high-grade glioma cell lines (A172, LN229 and SF539) and low expression in low-grade glioma (HS683) and normal (HMC3) cell lines, with statistically significant differences (Fig. 11D and E). Additionally, immunohistochemical stained images from the HPA database revealed positive staining for *TIMP1* in the high-grade glioma tissue, while low-grade glioma and normal human astrocyte tissues were *TIMP1*$^{-}$ (Fig. 11C). The results of the flow cytometry experiments showed that, compared with the si-NC group, knocking down *TIMP1* expression did not significantly affect the apoptosis cycle of LN229 and SF593 cells (Figs. 11I and S6A). However, colony formation assays demonstrated that, compared with the si-NC group, knockdown of the *TIMP1* gene by both *TIMP1* si-RNAs reduced the number of colonies in LN229 and SF539 cells (Fig. 11H and K). Consistent with the colony formation assay results, the results of the EdU experiment showed that the fluorescence intensity of both the si-*TIMP1*-1 and si-*TIMP1*-2 groups was lower than that of the si-NC group (P<0.01; Figs. 11L and S6B), indicating a decline in cell proliferation capability. Consistent results were also obtained in the CCK-8 assays (Fig. 11M). These experimental results confirmed that knocking down *TIMP1* expression inhibited the proliferation of LN229 and SF539 cells. Overall, the comprehensive analysis suggested that *TIMP1* may play a critical role in the development and progression of high-grade glioma and could serve as a potential biomarker for prognostic and therapeutic purposes.

Discussion

Cancer cells have a unique metabolism, which requires complex and diverse metabolic pathways to meet their specific needs such as for growth and invasion (37,38). Furthermore, metabolic changes and regulation can significantly impact the outcome of tumors (39). Research demonstrates that glioma tumors primarily rely on FAO to produce ATP and cytosolic NADPH, which provide essential energy to tumor cells (34). The precursors of signaling molecules that regulate important

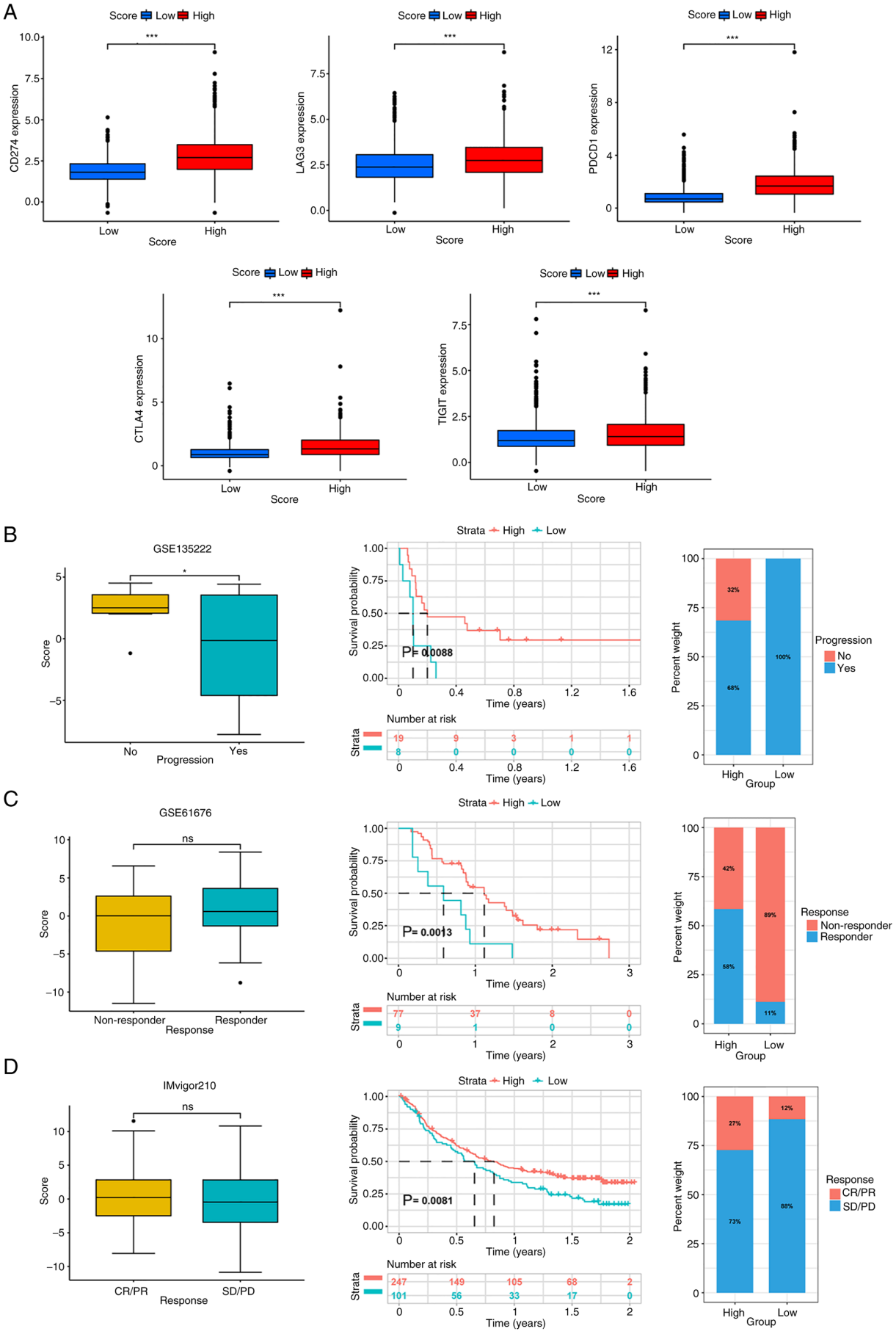

Figure 10. Relationship between the risk score model and the immunoparameters. (A) Difference in the expression of immune checkpoints in the high and low-risk scoring group. Validation of the immunotherapy score in the (B) GSE135222, (C) GSE61676 and (D) IMvigor210CoreBiologies external validation sets. *P<0.05, ***P<0.001; ns, not significant. CR, complete response; PD, progressive disease; PR, partial response; SD, stable disease.

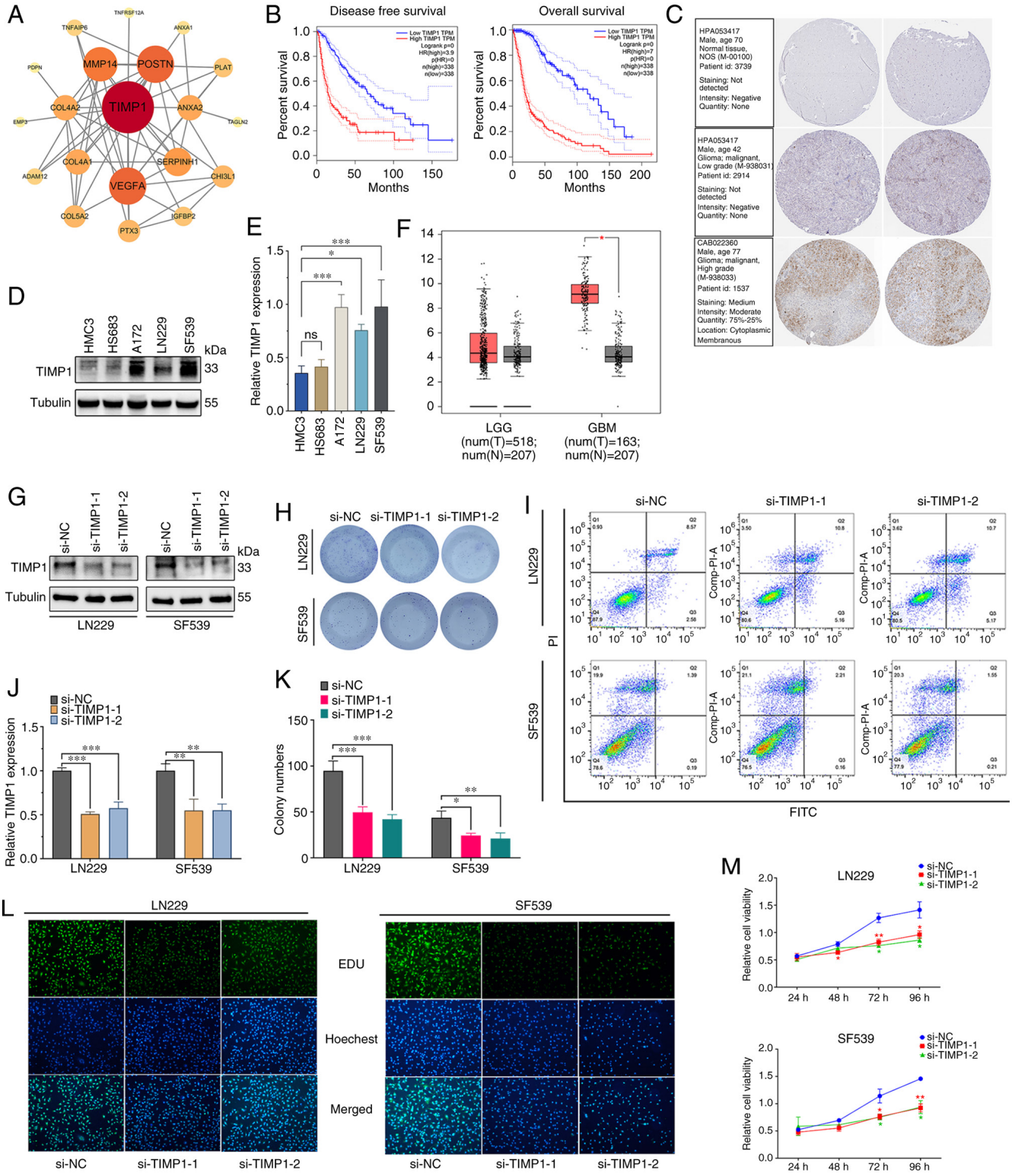

Figure 11. Validation of the DEGs and downregulation of *TIMP1*. (A) Protein-protein interaction network of the top 50 key DEGs. (B) Kaplan-Meier survival curve analysis of *TIMP1* in the glioma cohort. (C) *TIMP1* immunohistochemistry image from Human Protein Atlas database. (D) *TIMP1* expression levels in LGG and GBM. (E) WB and (F) semi-quantification experiments of *TIMP1* expression normal human astrocytes and glioma cell lines. Efficiency of *TIMP1* knockdown was confirmed by (G) WB and subsequently (H) semi-quantified. The results and statistics of (I) Colony formation assay in different transfection groups and subsequent (J) quantification. (K) Apoptosis of transfected LN229 and SF539 cells was assessed by flow cytometric assays. Proliferation of transfected LN229 and SF539 cells was assessed by (L) EdU and (M) Cell Counting Kit-8 assays. *P<0.05, **P<0.01, ***P<0.001. DEGs, differentially expressed genes; EdU, 5-ethynyl-2-doxyuridine; GBM, glioblastoma; HR, hazard ratio; LGG, low grade glioma; N, normal tissue; NC, negative control; si(RNA), small interfering (RNA); T, tumor tissue; TIMP1, tissue inhibitor of metalloproteinase 1; WB, western blotting.

biological processes of tumors are derived from FAs and their metabolic products. In addition, FAs play a pivotal role in ferroptosis, a non-traditional apoptosis mechanism, which is induced by the reaction of ferrous ions and reactive oxygen

species (ROS) (40). Moreover, the chemotherapy resistance, angiogenesis, metastasis and invasion of glioma cells are closely related to FA metabolism (41). Therefore, the occurrence and development of glioma heavily depend on FA metabolism. Previous studies have drawn attention to the immunosuppressive effects of FA metabolism on tumors. For instance, Miska *et al* (42) reported that etomoxir, an inhibitor of FA metabolism, inhibits the growth of MC38 tumor cells *in vivo*, which is dependent on preventing the immunosuppressive capabilities of $CD8^+$ and $CD4^+$ T cells. Similarly, Zhao *et al* (43) observed that FAO ultimately increases the tolerance of dendritic cells to enhance the resistance to immunotherapy in melanoma and generates tumor-regulatory T cells through indoleamine 2,3-dioxygenase-1 activity. In another study by Pearce *et al* (44), it was demonstrated that tumor necrosis factor receptor-associated factor 6 promotes FAO, which enhances the development of long-lived memory CD8 T cells. Notably, blocking FAO simultaneously boosts antitumor immunity and the efficacy of anti-programmed cell death protein 1 inhibitors (45).

Although some genes related to FA metabolism and the immune microenvironment of glioma have been experimentally verified, the research is still in its early stages and there is currently no effective method to target this pathway in clinical practice (14,46). Previous studies have used molecular markers related to FA metabolism to construct glioma prognosis models (33,34), but the link between the prognosis model and the tumor immune microenvironment remains unclear. Therefore, in the present study, a FAO-based model was comprehensively and systematically constructed to evaluate immune infiltration in patients with glioma and to discover the potential relationship and clinical value of FA metabolism and the immune microenvironment in glioma.

The findings of the present study revealed global changes in FAO-related genes in glioma cells at the transcriptional and genetic levels, which identified three distinct molecular clusters based on 13 FAO-related genes. Cluster B, associated with higher immune infiltration, displayed significantly worse prognosis, and other significant differences in the TME characteristics were observed between the clusters. The enrichment features of cluster B included the p53 signaling pathway, apoptosis, the ROS signaling pathway, DNA replication and mismatch repair. Pairwise comparison of three molecular clusters yielded 287 DEGs, and the clusters were further classified to two different gene subtypes based on the top 50 DEGs (rated according to the P-value). Patients with subtype B had a higher tumor grade, poor prognostic factors such as age, and a worse survival compared with patients with subtype A. Analysis of the clinicopathological information revealed poor prognostic indicators such as *IDH1* wild-type, 1p19q non-co-deletion and high tumor grade in the HSG. The expression of immune checkpoints was also generally higher in the HSG, indicating potential benefits with the administration of immune checkpoint inhibitors.

The scores from the model developed in the present study, by comparing the HSG and the LSG, demonstrated significantly different clinicopathological features, prognostic correlations, immune checkpoints and drug sensitivity. The scores were validated using an external validation set, and the immunotherapy response of the validation set could be predicted from this model. We consider that the findings of the present study provide critical insights into the molecular mechanisms of the role of FA metabolism in glioma and offer new ideas for drug development and targeted therapy.

In addition, the *TIMP1* gene was identified through key protein interactions in the current study. One study found that the expression of *TIMP1* in HT-29 colon adenocarcinoma cells increased the cell proliferation, migration and growth of tumor xenografts (47). Another study found that, among patients with endometrial cancer and breast cancer, patients with shorter recurrence times and later tumor stages were significantly positively correlated with the expression level of *TIMP1* (48,49). Numerous studies have also revealed the relationship between *TIMP1* and tumor progression and the TME (47-51). A recent study has also found that *TIMP1* is highly expressed in GBM, the *TIMP1* gene family is related to the immune infiltration of glioma and the immune response-related transcription factor, Sp1, can regulate the expression of *TIMP1* in GBM (45). The results of the present study further demonstrated the correlation between *TIMP1* expression and increased tumor proliferation. In addition, the key gene, *TIMP1*, was screened out to be included in the immune score of the developed model, and the score indicated a better immune response.. Furthermore, TIMP1 protein expression in different glioma cell lines was verified, and it was found that the expression level of TIMP1 increased with tumor grade. The present study, to the best of our knowledge, confirmed for the first time that the expression level of TIMP1 may be positively correlated with the degree of malignancy in glioma, which provided a further theoretical basis for the relationship between *TIMP1* and the growth, proliferation and immune infiltration of glioma. However, more immunohistochemical samples and *in vitro* experimental studies are required to verify this hypothesis.

In conclusion, the present study demonstrated that FAO-related genes are closely linked to glioma oncogenesis and progression, and that the clusters and scoring models constructed based on the FAO-related genes were effective in evaluating prognosis and immunotherapy response. FAO-related genes may be involved in one of the immune mechanisms of tumor development and therefore may be a new target for tumor treatment.

Acknowledgements

Not applicable.

Funding

This research was funded by the Guangxi Medical and Health Appropriate Technology Development and Promotion Project (grant no. S2020104).

Availability of data and materials

The datasets used and/or analyzed during the current study are available from the corresponding author on reasonable request.

Authors' contributions

YL contributed to data curation, conception and design, and was responsible for supervision. GL and ZZ were responsible

for supervision, writing the original draft of the manuscript and performing the formal analysis. FG was responsible for the methodology, performing the formal analysis and experiment, and review and editing the manuscript. LM and HP were responsible for data curation, the formal analysis, and writing, reviewing and editing the manuscript. All authors read and approved the final version of the manuscript. FG, LM and HP confirm the authenticity of all the raw data.

Ethics approval and consent to participate

Not applicable.

Patient consent for publication

Not applicable.

Competing interests

The authors declare that they have no competing interests.

References

1. Lapointe S, Perry A and Butowski NA: Primary brain tumours in adults. Lancet 392: 432-446, 2018.
2. Yang K, Wu Z, Zhang H, Zhang N, Wu W, Wang Z, Dai Z, Zhang X, Zhang L, Peng Y, *et al*: Glioma targeted therapy: Insight into future of molecular approaches. Mol Cancer 21: 39, 2022.
3. Weller M, van den Bent M, Preusser M, Le Rhun E, Tonn JC, Minniti G, Bendszus M, Balana C, Chinot O, Dirven L, *et al*: EANO guidelines on the diagnosis and treatment of diffuse gliomas of adulthood. Nat Rev Clin Oncol 18: 170-186, 2021.
4. Jiang T, Nam DH, Ram Z, Poon WS, Wang J, Boldbaatar D, Mao Y, Ma W, Mao Q, You Y, *et al*: Clinical practice guidelines for the management of adult diffuse gliomas. Cancer Lett 499: 60-72, 2021.
5. Stupp R, Taillibert S, Kanner A, Read W, Steinberg D, Lhermitte B, Toms S, Idbaih A, Ahluwalia MS, Fink K, *et al*: Effect of tumor-treating fields plus maintenance temozolomide vs maintenance temozolomide alone on survival in patients with glioblastoma: A randomized clinical trial. JAMA 318: 2306-2316, 2017.
6. Nicholson JG and Fine HA: Diffuse glioma heterogeneity and its therapeutic implications. Cancer Discov 11: 575-590, 2021.
7. Przybylowski CJ, Hervey-Jumper SL and Sanai N: Surgical strategy for insular glioma. J Neurooncol 151: 491-497, 2021.
8. Tan AC, Ashley DM, López GY, Malinzak M, Friedman HS and Khasraw M: Management of glioblastoma: State of the art and future directions. CA Cancer J Clin 70: 299-312, 2020.
9. Yeo AT, Rawal S, Delcuze B, Christofides A, Atayde A, Strauss L, Balaj L, Rogers VA, Uhlmann EJ, Varma H, *et al*: Single-cell RNA sequencing reveals evolution of immune landscape during glioblastoma progression. Nat Immunol 23: 971-984, 2022.
10. Wang LB, Karpova A, Gritsenko MA, Kyle JE, Cao S, Li Y, Rykunov D, Colaprico A, Rothstein JH, Hong R, *et al*: Proteogenomic and metabolomic characterization of human glioblastoma. Cancer Cell 39: 509-528.e20, 2021.
11. Bian X, Liu R, Meng Y, Xing D, Xu D and Lu Z: Lipid metabolism and cancer. J Exp Med 218: e20201606, 2021.
12. Martínez-Reyes I and Chandel NS: Cancer metabolism: Looking forward. Nat Rev Cancer 21: 669-680, 2021.
13. Pavlova NN, Zhu J and Thompson CB: The hallmarks of cancer metabolism: Still emerging. Cell Metab 34: 355-377, 2022.
14. Jiang N, Xie B, Xiao W, Fan M, Xu S, Duan Y, Hamsafar Y, Evans AC, Huang J, Zhou W, *et al*: Fatty acid oxidation fuels glioblastoma radioresistance with CD47-mediated immune evasion. Nat Commun 13: 1511, 2022.
15. Cheng X, Geng F, Pan M, Wu X, Zhong Y, Wang C, Tian Z, Cheng C, Zhang R, Puduvalli V, *et al*: Targeting DGAT1 ameliorates glioblastoma by increasing fat catabolism and oxidative stress. Cell Metab 32: 229-242.e8, 2020.
16. Martin-Perez M, Urdiroz-Urricelqui U, Bigas C and Benitah SA: The role of lipids in cancer progression and metastasis. Cell Metab 34: 1675-1699, 2022.
17. Puca F, Yu F, Bartolacci C, Pettazzoni P, Carugo A, Huang-Hobbs E, Liu J, Zanca C, Carbone F, Del Poggetto E, *et al*: Medium-chain acyl CoA dehydrogenase protects mitochondria from lipid peroxidation in glioblastoma. Cancer Discov 11: 2904-2923, 2021.
18. Bi J and Mischel PS: Acyl-CoA-binding protein fuels gliomagenesis. Cell Metab 30: 229-230, 2019.
19. Zhao Z, Zhang KN, Wang Q, Li G, Zeng F, Zhang Y, Wu F, Chai R, Wang Z, Zhang C, *et al*: Chinese glioma genome atlas (CGGA): A comprehensive resource with functional genomic data from Chinese glioma patients. Genomics Proteomics Bioinformatics 19: 1-12, 2021.
20. Liberzon A, Subramanian A, Pinchback R, Thorvaldsdóttir H, Tamayo P and Mesirov JP: Molecular signatures database (MSigDB) 3.0. Bioinformatics 27: 1739-1740, 2011.
21. Gentleman RC, Carey VJ, Bates DM, Bolstad B, Dettling M, Dudoit S, Ellis B, Gautier L, Ge Y, Gentry J, *et al*: Bioconductor: Open software development for computational biology and bioinformatics. Genome Biol 5: R80, 2004.
22. Sun D, Wang J, Han Y, Dong X, Ge J, Zheng R, Shi X, Wang B, Li Z, Ren P, *et al*: TISCH: A comprehensive web resource enabling interactive single-cell transcriptome visualization of tumor microenvironment. Nucleic Acids Res 49: D1420-D1430, 2021.
23. Canzler S and Hackermüller J: multiGSEA: A GSEA-based pathway enrichment analysis for multi-omics data. BMC Bioinformatics 21: 561, 2020.
24. Sotiriou C, Wirapati P, Loi S, Harris A, Fox S, Smeds J, Nordgren H, Farmer P, Praz V, Haibe-Kains B, *et al*: Gene expression profiling in breast cancer: understanding the molecular basis of histologic grade to improve prognosis. J Natl Cancer Inst 98: 262-272, 2006.
25. Laska E, Meisner M and Wanderling J: A maximally selected test of symmetry about zero. Stat Med 31: 3178-3191, 2012.
26. Kim JC, Heo YJ, Kang SY, Lee J and Kim KM: Validation of the combined biomarker for prediction of response to checkpoint inhibitor in patients with advanced cancer. Cancers (Basel) 13: 2316, 2021.
27. Zhang X, Shi M, Chen T and Zhang B: Characterization of the immune cell infiltration landscape in head and neck squamous cell carcinoma to aid immunotherapy. Mol Ther Nucleic Acids 22: 298-309, 2020.
28. Tu B, Ye L, Cao Q, Gong S, Jiang M and Li H: Identification of a five-miRNA signature as a novel potential prognostic biomarker in patients with nasopharyngeal carcinoma. Hereditas 159: 3, 2022.
29. Jung H, Kim HS, Kim JY, Sun JM, Ahn JS, Ahn MJ, Park K, Esteller M, Lee SH and Choi JK: DNA methylation loss promotes immune evasion of tumours with high mutation and copy number load. Nat Commun 10: 4278, 2019.
30. Baty F, Joerger M, Früh M, Klingbiel D, Zappa F and Brutsche M: 24 h-gene variation effect of combined bevacizumab/erlotinib in advanced non-squamous non-small cell lung cancer using exon array blood profiling. J Transl Med 15: 66, 2017.
31. Clough E and Barrett T: The gene expression omnibus database. Methods Mol Biol 1418: 93-110, 2016.
32. Braun DA, Hou Y, Bakouny Z, Ficial M, Sant' Angelo M, Forman J, Ross-Macdonald P, Berger AC, Jegede OA, Elagina L, *et al*: Interplay of somatic alterations and immune infiltration modulates response to PD-1 blockade in advanced clear cell renal cell carcinoma. Nat Med 26: 909-918, 2020.
33. Liu R, Liang W, Hua Q, Wu L, Wang X, Li Q, Zhong F, Li B and Qiu Z: Fatty acid metabolic signaling pathway alternation predict prognosis of immune checkpoint inhibitors in glioblastoma. Front Immunol 13: 819515, 2022.
34. Lin H, Patel S, Affleck VS, Wilson I, Turnbull DM, Joshi AR, Maxwell R and Stoll EA: Fatty acid oxidation is required for the respiration and proliferation of malignant glioma cells. Neuro Oncol 19: 43-54, 2017.
35. Otasek D, Morris JH, Bouças J, Pico AR and Demchak B: Cytoscape automation: Empowering workflow-based network analysis. Genome Biol 20: 185, 2019.
36. Xu H, Zhang Y, Liu J, Cui J, Gan Y, Wu Z, Chang Y, Sui R, Chen Y, Shi J, *et al*: UM-164, a dual inhibitor of c-Src and p38 MAPK, suppresses proliferation of glioma by reducing YAP activity. Cancers (Basel) 14: 5343, 2022.

37. Luis G, Godfroid A, Nishiumi S, Cimino J, Blacher S, Maquoi E, Wery C, Collignon A, Longuespée R, Montero-Ruiz L, *et al*: Tumor resistance to ferroptosis driven by Stearoyl-CoA Desaturase-1 (SCD1) in cancer cells and fatty acid biding protein-4 (FABP4) in tumor microenvironment promote tumor recurrence. Redox Biol 43: 102006, 2021.
38. Wu L, Zhang X, Zheng L, Zhao H, Yan G, Zhang Q, Zhou Y, Lei J, Zhang J, Wang J, *et al*: RIPK3 orchestrates fatty acid metabolism in tumor-associated macrophages and hepatocarcinogenesis. Cancer Immunol Res 8: 710-721, 2020.
39. Ma Y, Temkin SM, Hawkridge AM, Guo C, Wang W, Wang XY and Fang X: Fatty acid oxidation: An emerging facet of metabolic transformation in cancer. Cancer Lett 435: 92-100, 2018.
40. Juraszek B, Czarnecka-Herok J and Nałęcz KA: Glioma cells survival depends both on fatty acid oxidation and on functional carnitine transport by SLC22A5. J Neurochem 156: 642-657, 2021.
41. Strickland M and Stoll EA: Metabolic reprogramming in glioma. Front Cell Dev Biol 5: 43, 2017.
42. Miska J, Lee-Chang C, Rashidi A, Muroski ME, Chang AL, Lopez-Rosas A, Zhang P, Panek WK, Cordero A, Han Y, *et al*: HIF-1α is a metabolic switch between glycolytic-driven migration and oxidative phosphorylation-driven immunosuppression of Tregs in glioblastoma. Cell Rep 27: 226-237.e4, 2019.
43. Zhao F, Xiao C, Evans KS, Theivanthiran T, DeVito N, Holtzhausen A, Liu J, Liu X, Boczkowski D, Nair S, *et al*: Paracrine Wnt5a-β-catenin signaling triggers a metabolic program that drives dendritic cell tolerization. Immunity 48: 147-160.e7, 2018.
44. Pearce EL, Walsh MC, Cejas PJ, Harms GM, Shen H, Wang LS, Jones RG and Choi Y: Enhancing CD8 T-cell memory by modulating fatty acid metabolism. Nature 460: 103-107, 2009.
45. Wang T, Fahrmann JF, Lee H, Li YJ, Tripathi SC, Yue C, Zhang C, Lifshitz V, Song J, Yuan Y, *et al*: JAK/STAT3-regulated fatty acid β-oxidation is critical for breast cancer stem cell self-renewal and chemoresistance. Cell Metab 27: 136-150.e5, 2018.
46. Zhan Y, Qiao W, Yi B, Yang X, Li M, Sun L, Ji L, Su P, Wang X, Zhang F, *et al*: Dual role of pseudogene TMEM198B in promoting lipid metabolism and immune escape of glioma cells. Oncogene 41: 4512-4523, 2022.
47. Song G, Xu S, Zhang H, Wang Y, Xiao C, Jiang T, Wu L, Zhang T, Sun X, Zhong L, *et al*: TIMP1 is a prognostic marker for the progression and metastasis of colon cancer through FAK-PI3K/AKT and MAPK pathway. J Exp Clin Cancer Res 35: 148, 2016.
48. Yi YC, Chen MK, Chen LY, Ho ES, Ying TH, Wang PH and Yang SF: Genetic polymorphism of the tissue inhibitor of metalloproteinase-1 is associated with an increased risk of endometrial cancer. Clin Chim Acta 409: 127-131, 2009.
49. Eiro N, González L, Martínez-Ordoñez A, Fernandez-Garcia B, González LO, Cid S, Dominguez F, Perez-Fernandez R and Vizoso FJ: Cancer-associated fibroblasts affect breast cancer cell gene expression, invasion and angiogenesis. Cell Oncol (Dordr) 41: 369-378, 2018.
50. Tian Z, Ou G, Su M, Li R, Pan L, Lin X, Zou J, Chen S, Li Y, Huang K and Chen Y: TIMP1 derived from pancreatic cancer cells stimulates schwann cells and promotes the occurrence of perineural invasion. Cancer Lett 546: 215863, 2022.
51. Yang L, Jiang Q, Li DZ, Zhou X, Yu DS and Zhong J: TIMP1 mRNA in tumor-educated platelets is diagnostic biomarker for colorectal cancer. Aging (Albany NY) 11: 8998-9012, 2019.